

Constructing quantum many-body scar Hamiltonians from Floquet automata

Pierre-Gabriel Rozon,¹ Michael J. Gullans,² and Kartiek Agarwal¹

¹*Physics Department, McGill University, Montréal, Québec H3A 2T8, Canada**

²*Joint Center for Quantum Information and Computer Science,
NIST/University of Maryland, College Park, Maryland, 20742 USA*

(Dated: December 24, 2021)

We provide a systematic approach for constructing approximate quantum many-body scars (QMBS) starting from two-layer Floquet automaton circuits that exhibit trivial many-body revivals. We do so by applying successively more restrictions that force local gates of the automaton circuit to commute concomitantly more accurately when acting on select scar states. With these rules in place, an effective local, Floquet Hamiltonian is seen to capture dynamics of the automata over a long prethermal window, and neglected terms can be used to estimate the relaxation of revivals. We provide numerical evidence for such a picture and use our construction to derive several QMBS models, including the celebrated PXP model.

Understanding how thermalization arises from unitary evolution remains a fundamental challenge in the study of non-equilibrium quantum dynamics. The Eigenstate Thermalization Hypothesis [1, 2] (ETH) postulates that eigenstates of many-body quantum systems themselves encode thermal correlations when viewed by a local observer. Although ETH has been numerically verified in a wide variety of quantum systems [3–5], several important exceptions are known that challenge its associated dogma. The most prominent of these are integrable systems which occur in models with fine-tuned parameters [6], and many-body localized systems [7–10] where more robust local integrals of motion [11] emerge due to strong disorder. These systems exhibit a lack of level repulsion at all energies, a hallmark of non-ergodicity, and have certain persistent quantum correlations [12–14].

More recently, an experiment in a Rydberg atom chain found dramatic revivals in many-body quantum correlations after apparent relaxation, only when the system is initialized in *specific states* [15]. It is now understood that certain quantum systems can break ergodicity weakly [16], by only violating ETH over a sub-extensive number of eigenstates. These systems have been dubbed quantum many-body scars [17] (QMBS),

generalizing the phenomenon well known in the single-particle setting [18]. Since the initial findings, low entanglement eigenstates in the middle of the spectrum have been discovered in well known models [19, 20] and a number of theoretical proposals for constructing new QMBS Hamiltonians have been put forth, with the aid of spectrum generating algebras [21–24], projective constructions [25], matrix product state representations [26], among others; see Ref. [27] for a more exhaustive list of references.

Crucially, these proposals yield Hamiltonians that exhibit *exact* QMBSs, accompanied by perfect, indefinite revivals in correlations. This is in contrast to the original experimentally motivated PXP model [16, 17, 28] that exhibits imperfect revivals that decay at long times. Although weak perturbations may be added to exact QMBSs to obtain such decay, it remains a challenge to explain the existence of QMBS Hamiltonians such as the PXP model that have no small parameter, as well as uncover what sets the timescale for the decay of quantum revivals.

In this work, we illustrate general principles to derive approximate QMBSs without any small parameters from Floquet automaton circuits. We further show how a timescale for the decay of revivals naturally emerges in this setting. Floquet automata are unitary circuits that effect permutations of computational basis states on a chain of qubits. They are naturally associated with systems with state space [29–31] or kinetic constraints [32–35] and can exhibit non-trivial dynamical features in both the classical [36] and quantum settings [37–40]. The Hilbert space is fragmented into disjoint subspaces of computational basis states which are cycled through with successive applications of the automata circuit, reviving at fixed time intervals. It is natural to ask if they can be used to construct QMBS Hamiltonians which show similar revivals. We find that the answer is yes, and the principles derived can be used to obtain, for instance, the PXP model, besides several new QMBS models we propose.

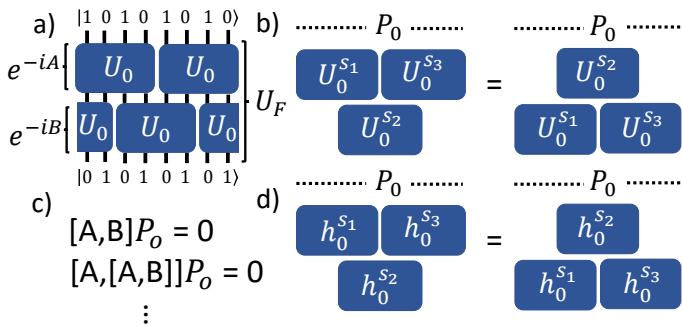


FIG. 1. a) An automaton circuit that converts one Néel state to another; b) and d) Local commutation rules of Type I and II respectively enforced on the orbit subspace; c) Global rules.

For concreteness, we focus on automata with a two-layer brickwork circuit [illustrated in Fig. 1 (a)] composed of the elementary gate U_0 and whose Floquet unitary is given by $U_F = e^{-iA}e^{-iB}$, where A, B are local Hamiltonians related by translation. A naive application of the Baker-Campbell-Hausdorff (BCH) formula to obtain a Hamiltonian from U_F is bound to fail as higher order commutators blow up in amplitude quickly while growing more non-local. Instead, we ask when the local Hamiltonian, $H_{\text{eff}} = A + B$, can reproduce dynamics generated by U_F on a *subspace* of chosen ‘orbit’ states, by virtue of forcing higher-order commutators to remain small (or vanish) in this subspace. In particular, defining $C_n(A, B)$ as the n^{th} order term in the expansion, we formulate rules that strongly suppress $\|C_n(A, B)P_o\|$, where P_o is the projector onto the orbit subspace. Note that this bounds both $\|P_o C_n P_o\|$, which governs the corrections to the dynamics within the subspace of orbit states, and $\|(1 - P_o)C_n P_o\|$, which governs the leakage from the orbit states into ‘generic’ states.

The rules we impose on U_0 come in two broad categories—i) commutators of U_0 or $h_0 \equiv i \log U_0$ vanish locally (and consequently, globally) on the orbit subspace, or ii) intricate phase relations between local gates allow for non-zero local commutators (even on the orbit subspace) but force the global commutator, $\|C_n P_o\|$, to vanish nonetheless. In the first category, we find that successively implementing more rules that further suppress the norm of C_n gives rise to H_{eff} with longer lived revivals. We illustrate this explicitly by constructing the ‘QMBS-A/B/C’ models which successively show stronger revivals with QMBS-C being an exact QMBS. We also confirm that the PXP model falls into this category and can be obtained from a Floquet automaton composed of Toffoli gates [40], and exhibits strong suppression of higher order BCH terms when projected on to the subspace of Néel states. In the second category, we propose another model ‘QMBS-G’ that shows incredibly long revivals. All models studied are found to exhibit level-repulsion, and, thus, appear to be non-integrable.

Besides allowing us to find new non-trivial QMBSs, the reference to automata also sheds light on the possible mechanism of decay of revivals in imperfect QMBSs. Two putative timescales emerge—i) the terms neglected in H_{eff} give rise to leakage from ideal automata transition between orbit states, and this is captured by a timescale τ_l governed by the inverse of $\|(1 - P_o)C_n P_o\|$, and ii) a prethermal timescale that justifies the truncation of H_{eff} to finite order—although the rules are designed to suppress BCH terms governing dynamics on orbit states (and leakage), they eventually grow at some higher order. In QMBS-G and PXP models, we find that BCH terms initially *decrease* with increasing order n , characteristic of the amplitude of terms in the Floquet-Magnus (FM) expansion [41] with an effective drive period $T < 1$. This behavior is suggestive of a prethermalization [42–45] win-

dow $\tau_p \sim e^{1/T}$ wherein a truncated Hamiltonian can be justified. The parameter T is an emergent scale that comes from the suppression of commutators and is not intrinsic to the two two-layer automaton which has a unit drive period. In this case, adding small, higher order BCH terms improves revivals, and the absence of these in H_{eff} can be understood as the small perturbation that leads to decay of revivals at a timescale τ_l . The picture is more complex for QMBS-A and QMBS-B which we elaborate upon later.

Local Rules of Type I and models QMBS-A/B/C— Without allowing for the possibility of phases, the space of permutations alone on 4 qubits is $16!$ and difficult to exhaustively search for all possible U_0 with suppressed $\|C_n(A, B)P_o\|$. Moreover, the latter depends on the explicit choice of P_o , or the orbit states. For concreteness, in all models we consider except PXP, we focus on i) U_F that have an orbit that cycles between the two Néel states as shown in Fig. 1, ii) $U_0^l = \mathbb{1}$ for some small l , and iii) periodic boundary conditions.

The condition $U_0^l = \mathbb{1}$ ensures that the Hamiltonian for one layer of the circuit, $A = \sum_i A_i$, with $A_i = i \log(U_{0,i})$ can be represented in powers of U_0 up to l . $\|C_n P_o\|$ then vanish if all independent powers of U_0 commute with each other locally on the orbit subspace, as shown in Fig. 1 (b), and proven exhaustively in the Supplemental Material (SM). Choosing U_0 that satisfy all these rules results in perfect revivals as the dynamics on the subspace of orbit states is then *exactly* given by $H_{\text{eff}} = A + B$. When only some of the above rules are satisfied, one finds imperfect revivals that exhibit decay over long times.

In particular, we consider $U_0^6 = \mathbb{1}$ and look at possible U_0 that satisfy the rules [Fig. 1 (b)] partially. To constraint our search, we additionally assume that U_0 acts as identity on the rightmost qubit. Searching over all possible $8!$ permutation unitaries (with no dynamical phase), we find three example models, QMBS-A,B,C, which satisfy 110/350, 246/350 and all of the rules applicable, respectively [46]. As intuitively expected, QMBS-B shows stronger and longer lasting revivals compared to QMBS-A. The exact scar model QMBS-C supports a spectrum generating algebra like many other exact QMBS models; see SM for more details.

Local Rules of Type II and PXP Model.— The PXP model is also closely related to an automaton, as pointed out in Ref. [40]. The PXP automaton can be described as a two-layer circuit with three-qubit Toffoli gates U_T that effect the orbit $|010101\dots\rangle \rightarrow |111111\dots\rangle \rightarrow |101010\dots\rangle \rightarrow |010101\dots\rangle$ and satisfy $U_T^4 = \mathbb{1}$. Note that it is important to include a phase in the definition of the Toffoli gates to obtain the correct (PXP) Hamiltonian from H_{eff} —without this phase a related model is obtained which exhibits much weaker revivals; see SM.

The PXP automaton satisfies a different set of local rules—although local gates U_T do not commute with each other on the orbit subspace, the local terms of the

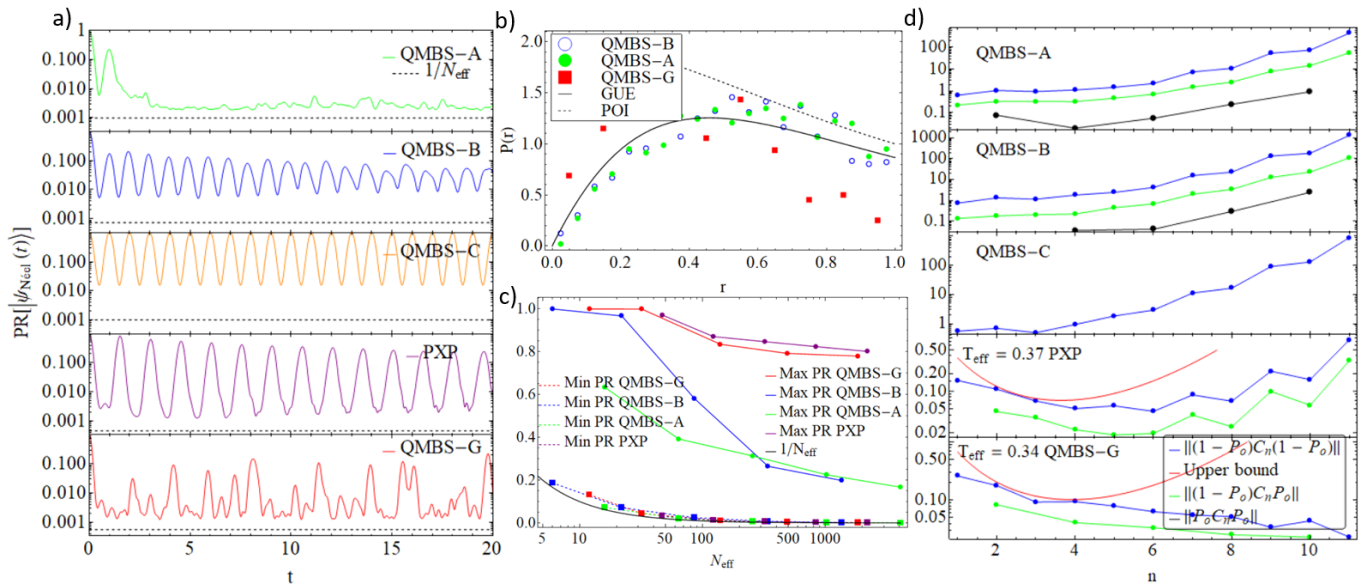


FIG. 2. (a) Revivals of the Néel state as seen from the PR of the time-evolved state for the various models studied. (b) Non-integrability of all models can be seen in the suppression of $P(r)$ at small values of the r -statistic. (c) The maximum and minimum IPR of evolved wavefunction in the time range $t \in (1, 300)$ versus dimension of effective Hilbert space. The minimum closely follows the inverse Hilbert space dimension (black line) (d) Leakage from orbit states, characterized by $\|(1 - P_0)C_n P_0\|$ (green), from n^{th} order BCH term neglected in H_{eff} , and norm of the neglected terms projected to the subspace of generic states (blue) and orbit states (black). Missing points/lines indicate corresponding zero values. Red lines show norm of FM expansion at effective drive period T indicated.

Hamiltonian, given by $h_T \equiv i \log U_T = \text{PXP}$ do commute for the most part. Indeed, local rules of Type I can be formulated in an alternate way—by requiring various powers of h_0 to commute locally; see Fig. 1 (d). Here we can restrict the search to those automata for which $\{h_0^l\}, l \in \mathbb{Z}^+$ form a finite set of independent operators, in order that commutation rules can be better enforced. Although we do not perform an exhaustive search over such U_0 , we note that the PXP model comes in this category, with only h_T, h_T^2 being independent, and remarkably, the PXP model satisfies all local commutation rules except breaking a single rule on a single orbit state. Note, additionally that the advantage of working with rules of type II (and thus, limiting commutators of h_0 instead of U_0) is that the BCH expansion becomes an expansion in a small parameter associated with the decay of revivals.

Global Rules and model QMBS-G.— A final possibility is that the unitary gate U_0 does not satisfy local rules in either incarnation [Fig. 1 (b) or (d)] but instead, is devised such that only the extensive terms A, B satisfy $\|C_n(A, B)P_0\| = 0$. This requires an intricate relationship between terms generated by local commutators $[h_{0,i}, h_{0,i+2}]$ and their associated phases. We present one example of such a model which we term QMBS-G that was designed by deforming QMBS-C minimally—without impacting the transition from one Néel state to the other in the associated automaton, while forcing $\|C_1(A, B)P_0\| = 0$. The model appears to also have

highly suppressed higher order BCH terms. The unitaries U_0 for all the models presented are explicitly stated in SM.

Numerical data.— We now discuss numerical simulation of these models. For all models, we consider periodic boundary conditions and system sizes L such that the effective Hilbert space dimension N , of states accessible dynamically from Néel states (obtained numerically), is > 1000 for the largest L studied—this corresponds to $L = 24$ for QMBS-G, $L = 16$ for PXP, and $L = 12$ for QMBS-A/B. In Fig. 2 (a), we look at the revivals by examining the participation ratio (PR) of the time-evolved state $|\psi_{\text{Néel}}(t)\rangle$ starting from the Néel state at time $t = 0$. The PR is evaluated in the basis of computational basis states $|i\rangle = |001010\dots\rangle$, as $\text{PR} [|\psi\rangle] = \sum_i |\langle i | \psi \rangle|^4 / (\sum_i |\langle i | \psi \rangle|^2)^2$. A PR close to 1 indicates that the system is largely in one computational basis state while a PR $\sim 1/N$ implies relaxation. In the models QMBS-A/B/C derived using local rules of type I, we find a clear progression towards more long lived revivals as more local commutation rules are respected. The PXP and QMBS-G models show remarkably strong revivals although the latter exhibits rather erratic and unpredictable times at which the revival occurs.

In Fig. 2 (b), we look at the level statistics of all models studied to confirm that they are indeed non-integrable (except for the perfect scar model QMBS-C which is explicitly integrable in the subspace of inter-

est). All models exhibit level repulsion seen as a suppression in the distribution $P(r)$ at small values of the r -statistic, obtained as the ratio of the minimum to the maximum energy differences between successive eigenstates, $r_i = \max[\delta_i, \delta_{i+1}] / \min[\delta_i, \delta_{i+1}]$. Note, QMBS-A/B appear to closely follow GUE predictions. $P(r)$ remains jagged for QMBS-G at the largest system size accessible despite aggregating data over large bins of size $\delta r = 0.1$; nevertheless, we find clear evidence of level repulsion at small r and expect the model to be non-integrable. In Fig. 2 (c), we examine the finite-size scaling of the revivals in the PR of the time-evolved Néel state. The minima appear to coincide well with inverse Hilbert space dimension $\sim 1/N$, indicating near complete relaxation at intermediate times. The maxima corresponding to revivals, on the other hand, decrease with increasing system size but only as $-\log(N)$ suggesting that the phenomena may be robust in the thermodynamic limit. In SM, we show the inverse-PR of eigenstates of these models as a function of their energy and see evidence of low inverse-PR states at roughly equal energies in all models.

Finally, we look at the normalized operator norm of the BCH expansion terms C_n when projected into the subspace of orbit states and generic states in Fig. 2(d). Specifically, we compute $\|P_o C_n P_o\|$, $\|(1 - P_o) C_n (1 - P_o)\|$ and $\|(1 - P_o) C_n P_o\|$ to quantify the amplitude of neglected terms that govern dynamics within the orbit subspace (in the subspace of generic states) and lead to leakage from orbit states to generic states, respectively. Here, P_o is the projector onto the Néel states, and $\|X\|$ is the operator norm of X normalized by the operator norm of the zeroth order term, $A + B$, which is $\leq (L/2)\pi, L\pi$ for the 4 qubit gate models and the PXP model, respectively. We also compare this to the norm of the terms in the Floquet-Magnus (FM) expansion [42] with an effective drive period T for QMBS-G and PXP models.

Timescale for relaxation of revivals. — Figure 2 (d) summarizes some of our key findings. For all models of QMBSs we propose, all these terms are indeed small with $\|(1 - P_o) C_1 P_o\|, \|P_o C_1 P_o\|$ being at least an order of magnitude or two smaller than the zeroth order term, if it does not vanish exactly. Specifically in QMBS-G and PXP models, the norm of BCH terms first *decreases* with n before eventually increasing (at least for PXP). This is characteristic of the FM expansion for systems driven at high frequencies and which thus possess a prethermal window [41, 42, 44] of duration $\tau_p \sim e^{1/T}$ over which an effective Floquet Hamiltonian can be obtained by truncating the FM expansion. We find evidence of such prethermal behavior by examining the decay of $\langle \sigma_i^z(t) \rangle^2$ starting from a generic computational basis state; the revivals of the state quickly vanish, particularly in the PXP, but the local operator continues to have long revivals—see Fig. 3. Furthermore, adding BCH terms to H_{eff} for QMBS-G and PXP models improves revivals; see SM.

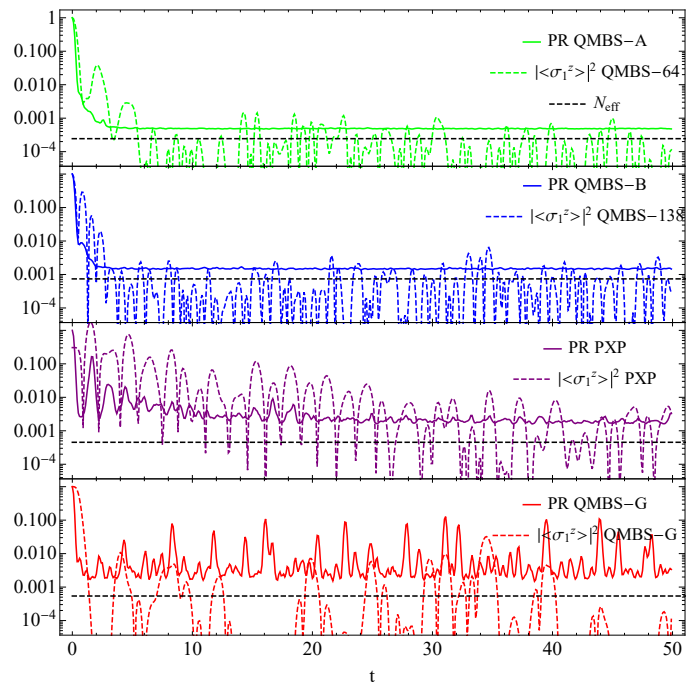


FIG. 3. PR of generic states evolved in time and expectation value squared of the local operator σ_z in this state.

Thus, we can think of the absence of such BCH terms in H_{eff} as a perturbation away from the ideal Floquet automaton which leads to the decay of revivals. Then, $\|(1 - P_o) C_1 P_o\|^2 L\pi/4$ can be understood as a Fermi's Golden Rule rate of decay of revivals and estimated to be $\tau_l \sim 1000$ for both QMBS-G and PXP models. Note, for QMBS-G and PXP models, the terms within the Néel subspace are also small for reasons of locality (which prevents C_n from leading to transitions between Néel states) and symmetry (which prevents an energy offset between the Néel states due to particle-hole symmetry in QMBS-G and translational symmetry in PXP). The latter likely aid stronger revivals and could be useful ingredients in searching for other approximate QMBS models using the methods we propose.

QMBS-C is an exact scar model where all BCH terms vanish exactly on the orbit subspace. Analyzing QMBS-A and QMBS-B is more subtle. Although it is clear that QMBS-B exhibits stronger revivals than QMBS-A and has a spectrum with equally spaced low-IPR states more akin to PXP, the BCH expansion for the two models has a similar behavior. Explicitly, adding more BCH terms to H_{eff} for these models does not improve revivals; see SM. This can be viewed as a consequence of forcing commutation of local unitary gates U_0 on the orbit subspace as opposed to the related h_0 in the derivation of these models. We anticipate an alternative expansion exists in powers of U_0 from which similar results (prethermalization window and leakage time) can be derived for these

models and requires further investigation.

Conclusions and Outlook.— This work demonstrates several deep connections between Floquet automata and non-thermalizing behavior in QMBSs. In particular, we show how i) perfect and imperfect QMBS Hamiltonians can be systematically constructed from Floquet automata by constraining the unitaries to satisfy certain commutation rules that protect orbit states and ii) that this approach recovers the small perturbation (corresponding to the deviation of the strictly local Floquet Hamiltonian from the quasilocal Floquet Hamiltonian that captures automaton dynamics over a prethermal window) that can be understood to give rise to the relaxation of QMBSs, despite these models lacking an obviously small parameter. The methods proposed can be used to rederive the seminal PXP model, besides several new models that we propose. Furthermore, such models are amenable to exploration in quantum simulation platforms, including for example Rydberg arrays [15], ion traps [14], and ensembles of defect spins in solids [47].

Acknowledgements.— The authors acknowledge useful discussions with Sarang Gopalakrishnan, Thomas Iadecola, Sanjaya Modugalya and Shivaji Sondhi. KA would like to acknowledge the hospitality of the Aspen Center for Physics where some of the ideas in this work were developed. PGR acknowledges graduate funding support from NSERC and FRQNT. MJG acknowledges support from the National Science Foundation (QLCI grant OMA-2120757). KA acknowledges funding support from NSERC, FRQNT, and the Tomlinson Scholar Award.

*

- [1] J. M. Deutsch, *Phys. Rev. A* **43**, 2046 (1991).
- [2] M. Srednicki, *Phys. Rev. E* **50**, 888 (1994).
- [3] M. Rigol, V. Dunjko, V. Yurovsky, and M. Olshanii, *Phys. Rev. Lett.* **98**, 050405 (2007).
- [4] M. Rigol, V. Dunjko, and M. Olshanii, *Nature (London)* **452**, 854 (2008).
- [5] H. Kim, T. N. Ikeda, and D. A. Huse, *Phys. Rev. E* **90**, 052105 (2014).
- [6] B. Sutherland, *Beautiful models: 70 years of exactly solved quantum many-body problems* (World Scientific, 2004).
- [7] D. Basko, I. Aleiner, and B. Altshuler, *Annals of Physics* **321**, 1126 (2006).
- [8] A. Pal and D. A. Huse, *Phys. Rev. B* **82**, 174411 (2010).
- [9] R. Nandkishore and S. Gopalakrishnan, arXiv preprint arXiv:1606.08465 (2016).
- [10] K. Agarwal, E. Altman, E. Demler, S. Gopalakrishnan, D. A. Huse, and M. Knap, *Annalen der Physik* **529**, 1600326 (2017).
- [11] D. A. Huse, R. Nandkishore, and V. Oganesyan, *Phys. Rev. B* **90**, 174202 (2014).
- [12] T. Kinoshita, T. Wenger, and D. S. Weiss, *Nature* **440**, 900 (2006).
- [13] M. Schreiber, S. S. Hodgman, P. Bordia, H. P. Lüschen, M. H. Fischer, R. Vosk, E. Altman, U. Schneider, and I. Bloch, *Science* **349**, 842 (2015).
- [14] J. Smith, A. Lee, P. Richerme, B. Neyenhuis, P. W. Hess, P. Hauke, M. Heyl, D. A. Huse, and C. Monroe, *Nature Physics* **12**, 907 (2016).
- [15] H. Bernien, S. Schwartz, A. Keesling, H. Levine, A. Omran, H. Pichler, S. Choi, A. S. Zibrov, M. Endres, M. Greiner, *et al.*, *Nature* **551**, 579 (2017).
- [16] C. J. Turner, A. A. Michailidis, D. A. Abanin, M. Serbyn, and Z. Papić, *Nature Physics* **14**, 745 (2018).
- [17] C. Turner, A. Michailidis, D. Abanin, M. Serbyn, and Z. Papić, *Physical Review B* **98**, 155134 (2018).
- [18] E. J. Heller, *Phys. Rev. Lett.* **53**, 1515 (1984).
- [19] S. Moudgalya, S. Rachel, B. A. Bernevig, and N. Regnault, *Physical Review B* **98**, 235155 (2018).
- [20] I. Affleck, T. Kennedy, E. H. Lieb, and H. Tasaki, in *Condensed Matter Physics and Exactly Soluble Models* (Springer, 2004) pp. 249–252.
- [21] S. Moudgalya, N. Regnault, and B. A. Bernevig, *Phys. Rev. B* **102**, 085140 (2020).
- [22] D. K. Mark, C.-J. Lin, and O. I. Motrunich, *Phys. Rev. B* **101**, 195131 (2020).
- [23] S. Choi, C. J. Turner, H. Pichler, W. W. Ho, A. A. Michailidis, Z. Papić, M. Serbyn, M. D. Lukin, and D. A. Abanin, *Phys. Rev. Lett.* **122**, 220603 (2019).
- [24] N. O’Dea, F. Burnell, A. Chandran, and V. Khemani, *Phys. Rev. Research* **2**, 043305 (2020).
- [25] N. Shiraishi and T. Mori, *Phys. Rev. Lett.* **119**, 030601 (2017).
- [26] W. W. Ho, S. Choi, H. Pichler, and M. D. Lukin, *Phys. Rev. Lett.* **122**, 040603 (2019).
- [27] S. Moudgalya, B. A. Bernevig, and N. Regnault, arXiv preprint arXiv:2109.00548 (2021).
- [28] M. Serbyn, D. A. Abanin, and Z. Papić, *Nature Physics* **17**, 675 (2021).
- [29] M. E. Fisher, *Physical Review* **124**, 1664 (1961).
- [30] C. L. Henley, *Annu. Rev. Condens. Matter Phys.* **1**, 179 (2010).
- [31] J. T. Chalker, *Topological Aspects of Condensed Matter Physics: Lecture Notes of the Les Houches Summer School: Volume 103, August 2014* **103**, 123 (2017).
- [32] G. H. Fredrickson and H. C. Andersen, *Physical review letters* **53**, 1244 (1984).
- [33] R. G. Palmer, D. L. Stein, E. Abrahams, and P. W. Anderson, *Physical Review Letters* **53**, 958 (1984).
- [34] J. Jäckle and S. Eisinger, *Zeitschrift für Physik B Condensed Matter* **84**, 115 (1991).
- [35] F. Ritort and P. Sollich, *Advances in physics* **52**, 219 (2003).
- [36] S. Wolfram, *Nature* **311**, 419 (1984).
- [37] S. Gopalakrishnan and B. Zakirov, *Quantum Science and Technology* **3**, 044004 (2018).
- [38] K. Klobas, B. Bertini, and L. Piroli, *Physical Review Letters* **126**, 160602 (2021).
- [39] J. W. Wilkinson, K. Klobas, T. Prosen, and J. P. Garahan, *Physical Review E* **102**, 062107 (2020).
- [40] T. Iadecola and S. Vijay, *Phys. Rev. B* **102**, 180302 (2020).
- [41] M. Bukov, L. D’Alessio, and A. Polkovnikov, *Advances in Physics* **64**, 139 (2015).
- [42] T. Mori, T. Kuwahara, and K. Saito, *Physical review letters* **116**, 120401 (2016).

- [43] T. Kuwahara, T. Mori, and K. Saito, *Annals of Physics* **367**, 96 (2016).
- [44] D. Abanin, W. De Roeck, W. W. Ho, and F. Huveneers, *Communications in Mathematical Physics* **354**, 809 (2017).
- [45] K. Agarwal and I. Martin, *Physical Review Letters* **125**, 080602 (2020).
- [46] The number of rules are given by $n(l-1)(l^2-1)$ where n is the number of orbit states.
- [47] G. Kucsko, S. Choi, J. Choi, P. C. Maurer, H. Zhou, R. Landig, H. Sumiya, S. Onoda, J. Isoya, F. Jelezko, E. Demler, N. Y. Yao, and M. D. Lukin, *Phys. Rev. Lett.* **121**, 023601 (2018).

SUPPLEMENTARY MATERIAL

Explicit form of U_0 for all models discussed

In this work, we studied local unitary matrices U_0 that act as a permutation on the computational basis states in addition to multiplying them by a phase. Each computational basis state can be assigned a number between 1 and 16 so that U_0 can be represented by a permutation and a phase map. The mapping of is done by interpreting the 1's and 0's used to represent the computational basis states in bra-ket notation as a decimal expansion in base 2, + 1. Explicitly,

$$\begin{aligned}
 |0000\rangle &\rightarrow 1, & |0001\rangle &\rightarrow 2, \\
 |0010\rangle &\rightarrow 3, & |0011\rangle &\rightarrow 4, \\
 |0100\rangle &\rightarrow 5, & |0101\rangle &\rightarrow 6, \\
 |0110\rangle &\rightarrow 7, & |0111\rangle &\rightarrow 8, \\
 |1000\rangle &\rightarrow 9, & |1001\rangle &\rightarrow 10, \\
 |1010\rangle &\rightarrow 11, & |1011\rangle &\rightarrow 12, \\
 |1100\rangle &\rightarrow 13, & |1101\rangle &\rightarrow 14, \\
 |1110\rangle &\rightarrow 15, & |1111\rangle &\rightarrow 16.
 \end{aligned} \tag{1}$$

We represent the phase map by an array of length 16 with the understanding that the i^{th} component of this array starting from the left is the complex number by which the i^{th} computational basis state is multiplied when acted upon by U_0 . Using this notation, we give the permutation cycle representation and the phase map of each U_0 studied in this work below.

$$\begin{aligned}
 U_{0,\text{QMBS-G}} &= ((1, 2), (4, 6), (7, 9), (8, 16), (10, 15), (11, 13)), \\
 \text{Ph}_{\text{QMBS-G}} &= (1, 1, 1, 1, 1, 1, 1, 1, 1, 1, -1, 1, -1, 1, 1).
 \end{aligned}$$

$$\begin{aligned}
 U_{0,\text{QMBS-B}} &= ((1, 15), (2, 16), (3, 9, 5), (4, 10, 6), (7, 13, 11), \\
 &\quad (8, 14, 12)),
 \end{aligned}$$

$$\text{Ph}_{\text{QMBS-B}} = (1, 1, 1, 1, 1, 1, 1, 1, 1, 1, 1, 1, 1, 1, 1).$$

$$\begin{aligned}
 U_{0,\text{QMBS-A}} &= ((1, 9), (2, 10), (3, 5, 15, 11, 13, 7), \\
 &\quad (4, 6, 16, 12, 14, 8)),
 \end{aligned}$$

$$\text{Ph}_{\text{QMBS-A}} = (1, 1, 1, 1, 1, 1, 1, 1, 1, 1, 1, 1, 1, 1, 1).$$

$$\begin{aligned}
 U_{0,\text{QMBS-C}} &= ((3, 5), (4, 6), (7, 15, 9), (8, 16, 10), (11, 13), \\
 &\quad (12, 14))
 \end{aligned}$$

$$\text{Ph}_{\text{QMBS-C}} = (1, 1, 1, 1, 1, 1, 1, 1, 1, 1, 1, 1, 1, 1, 1)$$

$$U_{0,\text{PXP}} = ((11, 15), (12, 16)),$$

$$\text{Ph}_{\text{PXP}} = (1, 1, 1, 1, 1, 1, 1, 1, 1, i, i, 1, 1, i, i).$$

Exact scar condition proof

Using the property that $U_0^l = I$, we can expand $i \log U_0$ as follows:

$$i \log U_0 = \sum_{j=0}^{l-1} c_j U_{0,4i-3}^j \tag{2}$$

for some set of coefficient c_i , which thus yield

$$A = -i \sum_{i=1}^{L/4} \sum_{j=0}^{l-1} c_j U_{0,4i-3}^j, \tag{3}$$

$$B = -i \sum_{i=1}^{L/4} \sum_{j=0}^{l-1} c_j U_{0,4i-1}^j. \tag{4}$$

Here we have included $-i$ in A, B for ease of notation. For this proof, the automaton unitary is thus $U_F = e^A e^B$.

Using the formal expansion of e^{A+B} ,

$$e^{A+B} = \sum_{i=0}^{\infty} \frac{(A+B)^i}{i!} \tag{5}$$

one can see that $e^{A+B} P_0$ will be equivalent to $e^A e^B P_0$ if all terms resulting from the expansion of $(A+B)^i$ in 5 can be rearranged as a product of B's on the right and A's on the left when acting on P_0 . This condition takes the form

$$A^{a_1} B^{a_2} A^{a_3} B^{a_4} \dots A^{a_{n-1}} B^{a_n} P_0 = A^{\sum_{i \in \text{odd}} a_i} B^{\sum_{i \in \text{even}} a_i} P_0, \tag{6}$$

where n and a_i can be any positive integers. Imposing $A^a B^b P_0 = B^b A^a P_0$ for any positive integers a and b will ensure that equation 6 is satisfied. Since A and B are sums of spatially decoupled unitary gates, powers of A and B will take the following form:

$$\begin{aligned}
 A^a &= \sum_{k_{0,1}+k_{0,5}+\dots+k_{l-1,L-3}=a} \binom{a}{k_{0,1}, k_{0,5}, \dots, k_{l-1,L-3}} \\
 &\quad (-ic_0 U_{0,1}^0)^{k_{0,1}} (-ic_0 U_{0,5}^0)^{k_{0,5}} \dots (-ic_{l-1} U_{0,L-3}^{l-1})^{k_{l-1,L-3}}
 \end{aligned} \tag{7}$$

and similarly for B. Here

$$\binom{a}{k_{0,1}, k_{0,5}, \dots, k_{l-1}, L-3}$$

represents the standard multinomial combinatorial function. From this expression, one can see that generic terms in an expansion of $A^a B^b$ will take the form

$$\prod_{i=1}^{L/4} U_{0,4i-3}^{\alpha_{4i-3}} \prod_{i=1}^{L/4} U_{0,4i-1}^{\alpha_{4i-1}} P_o \quad (8)$$

up to a multiplicative constant for some set of integers α_i including 0. Thus, in order to satisfy the identity $A^a B^b P_o = B^b A^a P_o$, it is sufficient to require that the expression

$$\prod_{i=1}^{L/4} U_{0,4i-3}^{\alpha_{4i-3}} \prod_{i=1}^{L/4} U_{0,4i-1}^{\alpha_{4i-1}} P_o = \prod_{i=1}^{L/4} U_{0,4i-1}^{\alpha_{4i-1}} \prod_{i=1}^{L/4} U_{0,4i-3}^{\alpha_{4i-3}} P_o \quad (9)$$

is satisfied, which is ensured by the commutation rules defined in the text. For the proof, see figure 4. If one replaces $\sum_j^{l-1} c_j U_{0,4i-1}^j$ by $i \log(U_{0,i})$ and performs an analogous derivation with $\log(U_{0,i})$ instead of $U_{0,i}$, imposing $\log(U_{0,i})^{s_1} \log(U_{0,i+4})^{s_3} \log(U_{0,i+2})^{s_2} P_o = \log(U_{0,i+2})^{s_2} \log(U_{0,i})^{s_1} \log(U_{0,i+2})^{s_3} P_o$ for some integers s_1, s_2 and s_3 , one can ensure that specific commutators of the BCH series vanish when applied to P_o . Tuning the phase of the $U_{0,i}$ gates wisely can, for example, make the first BCH term vanish when acting on P_o . We show how strongly this can affect the revival amplitude in figure 5. Finally, we note that in order to make BCH terms vanish, it is in principle not necessary to focus on local products of $\log(U_{0,i})$. Instead, one can take advantage of overlapping local terms in the BCH expansion to ensure that certain terms vanish when acting on the orbit subspace. This strategy was used to derive the QMBS-G model.

QMBS-C spectrum generating algebra

The local permutation corresponding to the perfect model is given by: ((3, 5), (4, 6), (7, 15, 9), (8, 16, 10), (11, 13), (12, 14)). The perfect scar obtained from this model is invariant under any modification of the 3 cycles or the 1 cycles. We thus consider for simplicity an effective permutation given by: ((3, 5), (4, 6), (11, 13), (12, 14)) = $U_{0,eff}$ where the phase map is assumed to be 1 on all computational basis states. The logarithm of this unitary can be expressed as a linear combination of the identity matrix and the unitary matrix $U_{0,eff}$, which yields:

$$h_{eff} = -\frac{\pi}{2} I + \frac{\pi}{2} U_{0,eff} \quad (10)$$

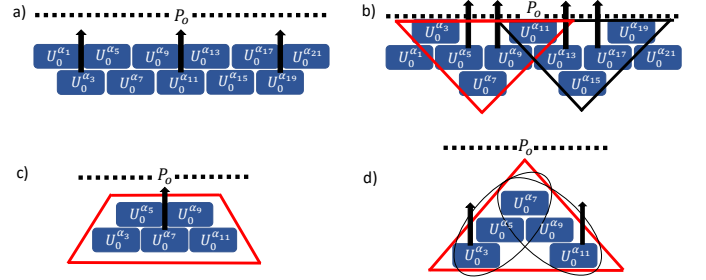


FIG. 4. a) We send specific gates from the second layer to the first layer. b) Within each decoupled triangle (here we focus on the red one), we commute specific gates from the first and second layer. c) Within the resulting configuration, we send the middle gate of the second layer to the first layer d) We send the side gates from the third layer to the first layer (Note that this is a 2 step operation for each side gate). The resulting arrangement of gates shows that by making use of the commutation rules, it is possible to send gate $U_0^{\alpha_7}$ from the third layer to the first layer in b). Repeating this procedure on each triangle proves the identity given in the text (i.e it will interchange the first and second layer in a))

We can further express $U_{eff,0}$ in terms of projectors and X gates

$$U_{eff,0,i} = P_i X_{i+1} X_{i+2} P_i + (I - P_i) \quad (11)$$

where P_i are given by

$$P_i = \frac{(I - Z_{i+1} Z_{i+2})}{2} \quad (12)$$

This yields for the Hamiltonian H_{eff}

$$H_{eff} = \frac{\pi}{2} \sum_{i=1}^{L/2} (P_{2i-1} X_{2i} X_{2i+1} P_{2i-1} - P_{2i-1}) \quad (13)$$

up to a constant. All terms in this Hamiltonian are decoupled in space. It gives rise to exact oscillation on a space composed of $2^{(L/2)}$ states. When including 3-cycles, one effectively embeds the above model in a larger subspace which can be completely thermalizing. (i.e we are free to choose any unitary we desire for the remaining degrees of freedom, as long as it only couples the following computational basis states: 8,16,10,7,15,9,1,2). We note that the model QMBS-G is expressed in the same effective subspace as QMBS-C (i.e the same $2^{(L/2)}$ states as in QMBS-C), but for QMBS-G this subspace is scrambling while still exhibiting special states with large revivals.

Obtaining QMBS-G

By examining QMBS-C, one can see that the transition rules are ensured by the 2-cycles ((4,6), (11,13)). It is then natural to ask if it is possible to obtain approximate

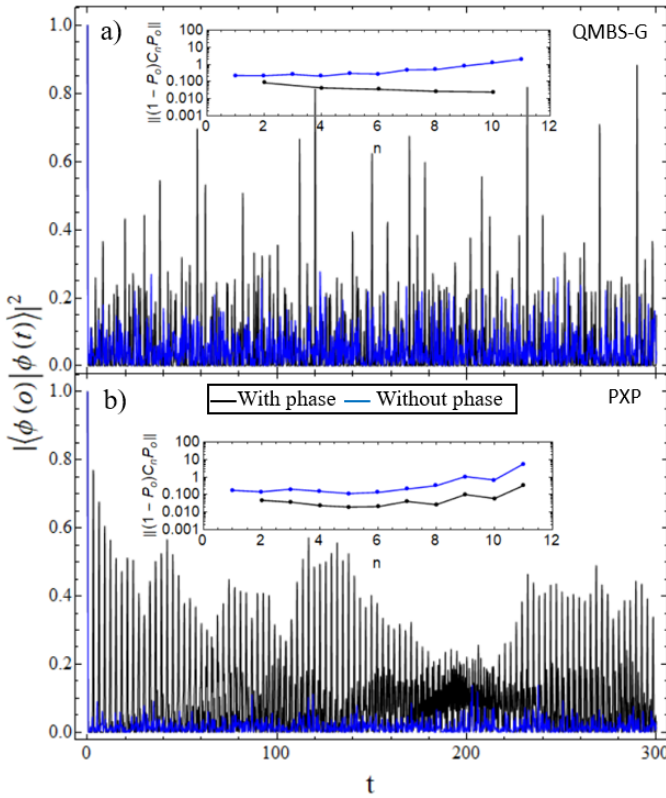


FIG. 5. Overlap amplitude squared of $|\psi_{\text{Neel}}(0)\rangle$ state with $e^{(A+B)t}|\psi_{\text{Neel}}(0)\rangle$ for models where we have trivial or non trivial phase. Insets show how the effective leakage changes between models with trivial and non-trivial phase.

scars by splitting the 2-cycles ((3,5), (12,14)) so that the resulting unitary is identity on those computational basis states. We further tune the phase of the states 3,5,12 and 14 in order to make the first commutator vanish when acting on orbit states by making use of interacting local commutators. The first BCH term C_1 is given by :

$$C_1 = \sum_{i=1}^{L/4} ([U_{0,4i-3}, U_{0,4i-1}] + [U_{0,4i-3}, U_{0,4i-5}]) \quad (14)$$

Up to a multiplicative constant. The action of the $i = 2$ term in C_1 on the Neel state $|10101010\dots\rangle$ yields :

$$\begin{aligned} & (U_{0,5}U_{0,7} - U_{0,7}U_{0,5} + \\ & U_{0,5}, U_{0,3} - U_{0,3}U_{0,5}) |10101010\dots\rangle = \\ & - |1010101100\dots\rangle - |1010110010\dots\rangle \quad (15) \\ & + |1011001010\dots\rangle + |1010110010\dots\rangle \\ & = - |1010101100\dots\rangle + |1011001010\dots\rangle \end{aligned}$$

Notice the sign change induced by the particular phase involved in $\text{Ph}_{\text{QMBS-G}}$. Similarly, the terms corresponding to arbitrary i will be the same, but translated in space. Because the Neel state maps to itself when translated by 2 sites, when adding all terms together, we end

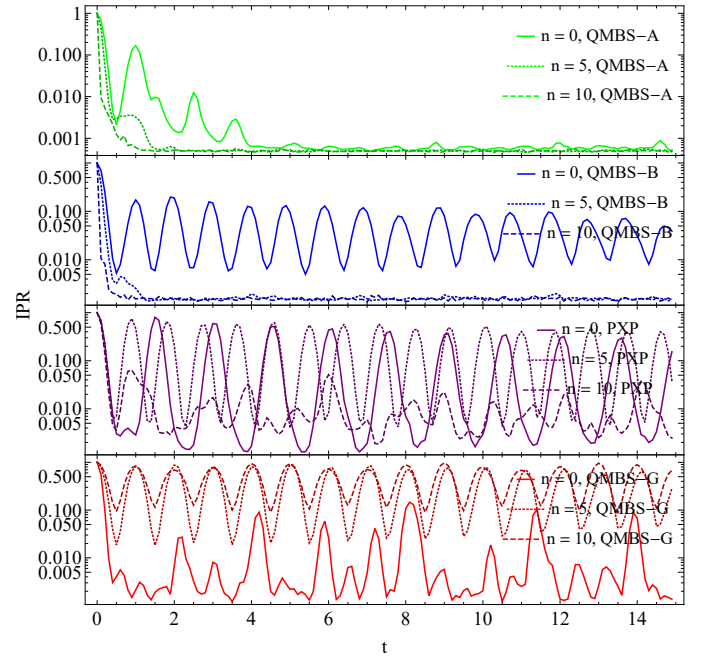


FIG. 6. Revivals seen in models with additional terms of order $l \leq n$ mentioned from the BCH expansion added to H_{eff} . Revivals improve when adding up to fifth order of BCH terms in the PXP model but worsen upon adding further higher orders, consistent with results for the BCH expansion seen in the main text. In contrast, revivals only improve upon adding further terms in QMBS-G, and only decrease when adding further terms in QMBS-A/B.

up adding the same computational basis states twice, but with opposite sign. With periodic boundary condition all terms cancel perfectly and the first BCH term vanishes when acting on P_0 .

PXP and QMBS-G with and without phase

As mentioned in the text, it is possible to impose commutation rules directly on h_0 in order to make specific BCH terms vanish when acting on the orbit subspace. Figure 5 highlights the flagrant difference in revival strength between related permutation model with trivial (phase is one for all computational basis states) and non-trivial phase. One can see that the former model exhibit smaller revivals which further corroborate the intuition that the amplitude of $\|(1 - P_0)C_n(P_0)\|$ is correlated with the strength of the revivals.

Other numerical evidence

In Fig. 6, we show evidence that revivals improve upon adding neglected higher order BCH terms to H_{eff} in the case of PXP and QMBS-G models, but make things worse

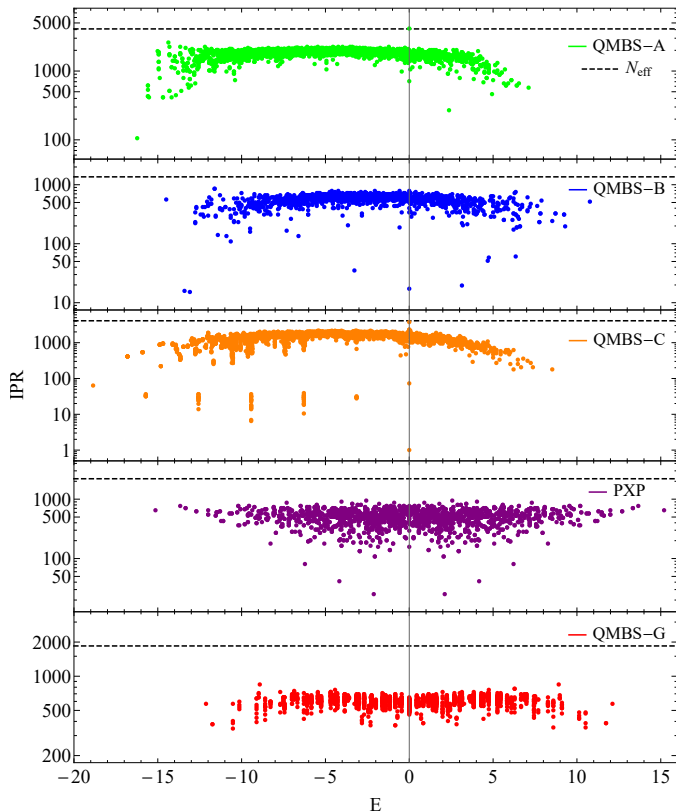


FIG. 7. Scatter plot of IPR vs. eigenstate energy in the 5 models studied in the main text. QMBS-B and QMBS-C (exact scar) clearly show more pronounced subspace of low IPR states compared to QMBS-A, which further seem to be separated equally in energy. Similar behavior is observed in the PXP model as well noted in Ref. [17]. QMBS-G show a thinner spread of states in terms of IPR along with bunching of energies into roughly equally spaced sectors.

for QMBS-A and QMBS-B. We anticipate that QMBS-A and QMBS-B can be interpreted within the context of a

different expansion which will show similar behavior to QMBS-G and PXP models.

Presence of low IPR states in the models

In Fig. 7, we plot the inverse participation ratio (IPR) against the energy of the eigenstates of the various models studied.

r-statistic and effective Hilbert space dimension.

In order to obtain the r-statistic distribution, we computed the r-values of each momentum sector independently and then combined the results to obtain a single distribution $P(r)$. We further removed exact degeneracies by suppressing r values that are exactly 0. The effective dimension of the models QMBS-A/B/C was computed numerically by time evolving the Néel state to large times and then finding numerically which computational basis states during the time evolution acquired a non-zero weight. For QMBS-G, the effective Hilbert space dimension was obtained by first restricting the Hilbert space to the space of $2^{(L/2)}$ states inherited for the connection to QMBS-C. This subspace was then refined numerically using the same method mentioned above. For PXP, we worked in the well known Fibonacci subspace, see [16]. The r-statistic was computed within the effective Hilbert space for all models. The maximum effective dimension we studied for each model is given by:

$$\begin{aligned}
 L = 16, N_{\text{PXP}} &= 2207 \\
 L = 12, N_{\text{QMBS-A}} &= 4096 \\
 L = 12, N_{\text{QMBS-B}} &= 1360 \\
 L = 12, N_{\text{QMBS-C}} &= 64 \\
 L = 24, N_{\text{QMBS-G}} &= 1848
 \end{aligned} \tag{16}$$